Dalton Transactions

ROYAL SOCIETY OF CHEMISTRY

PAPER

View Article Online
View Journal

Cite this: DOI: 10.1039/d6dt00630b

Structure–activity relationships of ATCUN-based Cu(II) complexes with large chelate rings: interplay of ROS generation, DNA binding, and nuclease activity

Julian Heinrich,[a,b] Johanna Lück,[b] Dmitrii Varlakhanov,[b,c] Ravi Kumar,[d] Matthias Stein [d] and Nora Kulak *[a,b]

Since the discovery of DNA cleavage and anticancer activity of the simplest Cu(II) ATCUN complex (peptide ligand: Gly–Gly–His, GGH) in 1983, systematic biological enhancements by derivatives have not been achieved. The stable 5,5,6-chelate ring structure provided by the original GGH ligand hampers efficient ROS production *via* Cu redox cycling (Cu(II/I)). In this work, we demonstrate that the incorporation of 7,5,6- and 7,6,6-chelates (Gly or β-alanine in the second peptide position, respectively) in combination with N-terminal design elements, such as γ-aminobutyric acid (GABA), 3,5-substituted (CF_3-, CH_3-) pyrazolyl and triazolyl units, provides an effective strategy to reinstate biological activity regarding ROS generation (determined *via* fluorescence spectroscopy and gel electrophoresis), DNA cleavage (gel electrophoresis) and DNA binding (fluorescence, UV/VIS and CD spectroscopy). Among the series of studied Cu(II) complexes, the metallopeptide with an amine group at the N-terminus (GABA) combined with a 7,6,6-chelate (β-alanine) system exhibits the highest overall biological activity, whereas a triazolyl moiety, independent of the chelate ring size (Gly: 7,5,6 and β-alanine: 7,6,6), leads to efficient hydroxyl radical generation. Computational studies based on an extensive conformational search of the metallopeptides, followed by an energy refinement at the level of Density Functional Theory (DFT), were used to elucidate the structure–activity relationship.

Received 15th March 2026,
Accepted 9th May 2026

DOI: 10.1039/d6dt00630b

rsc.li/dalton

Introduction

DNA is essential for protein biosynthesis in eukaryotic cells, and hence plays a fundamental role in the healthy function of cell proliferation.[1] Due to this fact, DNA is a promising target for chemotherapeutic agents in the clinical treatment of cancer.[2] The mode of action involves DNA dysfunction, which induces apoptosis, preferably in malignant cells.[3,4] Cisplatin is still one of the most commonly intravenously administered anticancer agents in chemotherapy since the discovery of its cytotoxicity in the 1970s.[5] This Pt-based metal complex causes irreversible DNA crosslinks through covalent metal bonding, which then consequently leads to DNA dysfunction and subsequently to apoptosis.[6] Disadvantages of the clinical application of cisplatin are severe side effects, such as nephro- and neurotoxicity, which are accompanied by a decrease in the quality of life of the cancer patient.[7] To overcome these harmful side effects of Pt-based chemotherapeutics current research is focused on anticancer compounds on the basis of endogenous metals, such as Cu and Fe, which may cause potentially lower systemic toxicity.[8,9]

It has been known for decades that redox-active Cu(II) complexes can produce reactive oxygen species (ROS). An external reducing agent, such as ascorbate ($AscH^-$, anion of vitamin C), initiates catalytic Cu(II)/Cu(I) redox cycling, which consequently leads to a cascade of ROS evolution (Scheme 1).[10–12] These

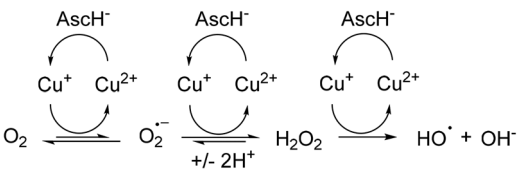

Scheme 1 Commonly accepted ROS generation for Cu(II) complexes. $AscH^-$ initiates the Cu(II)/Cu(I) redox cycling for ROS evolution.[12]

[a]*Institute of Chemistry, University of Potsdam, Karl-Liebknecht-Straße 24-25, 14476 Potsdam, Germany. E-mail: nora.kulak@uni-potsdam.de*
[b]*Institute of Chemistry, Otto von Guericke University, Universitätsplatz 2, 39106 Magdeburg, Germany*
[c]*Institute of Chemical Engineering and Technology, Kazan National Research Technical University, Ulitsa Karla Marksa 68, Kazan 420015, Russia*
[d]*Max Planck Institute for Dynamics of Complex Technical Systems, Sandtorstrasse 1, 39106 Magdeburg, Germany*

ROS potentially cause oxidative stress in cells[13] and are able to oxidatively cleave DNA, which is irreversible in the case of high nuclease activity. As a consequence, apoptosis is induced.[14] Such ROS-producing Cu(II) complexes are classified as artificial metallonucleases.[15,16] Furthermore, oxidative DNA damage/cleavage leads to potentially higher DNA dysfunction when compared to exclusive covalent Pt-DNA binding (DNA cross-links) of cisplatin, which makes Cu(II)-based metallonucleases a promising tool in cancer therapy.[16]

The amino-terminal Cu(II) and Ni(II) binding (ATCUN) motif is a 4N-chelating binding site for Cu(II) in natural proteins, such as albumins,[17] neuromedin C[18] and the Cu transport protein Ctr1.[19] At pH 7.4 Cu(II) is coordinated in a square planar fashion by the terminal amine group, two deprotonated peptide bonds and a δ-N of the imidazole moiety of His (Fig. 1, top).[20] For Cu(II) binding, His in the third position from the N-terminus is essential.[21] In 1983, a milestone was achieved by Linus Pauling and colleagues regarding the cytotoxic effect of such Cu(II) ATCUN peptide complexes. They reported that in the presence of $AscH^-$ the simplest ATCUN peptide ligand (NH_2–Gly–Gly–His–COOH = GGH) bound to Cu(II) (Fig. 1, top) exhibits high *in vivo* anticancer activity towards Ehrlich ascites tumor cells inoculated in mice, as well as *in vitro* oxidative DNA cleavage activity.[22,23]

However, over the following four decades, no significant improvements in bioactivity could be achieved through peptide sequence modifications,[24,25] except for an increase in antitumor activity *via* the introduction of targeting groups, such as acridine for G-quadruplex DNA.[26] A high complex stability ($\log K_{7.4}$ = 12.4) fixes the square planar Cu(II) geometry, which is caused by stable chelates within the complex structure (5,5,6), and consequently results in the inability to generate ROS, since the tetrahedral Cu(I) geometry is not accessible through $AscH^-$ activation (*cf.* Fig. 1, top and Scheme 1).[20,27] Over the decades, this fact led to neglecting Cu(II) ATCUN peptide complexes as promising chemotherapeutic candidates.[28] Nevertheless, we recently demonstrated that an exchange of the α-amino acid Gly for the β-amino acid β-Ala in

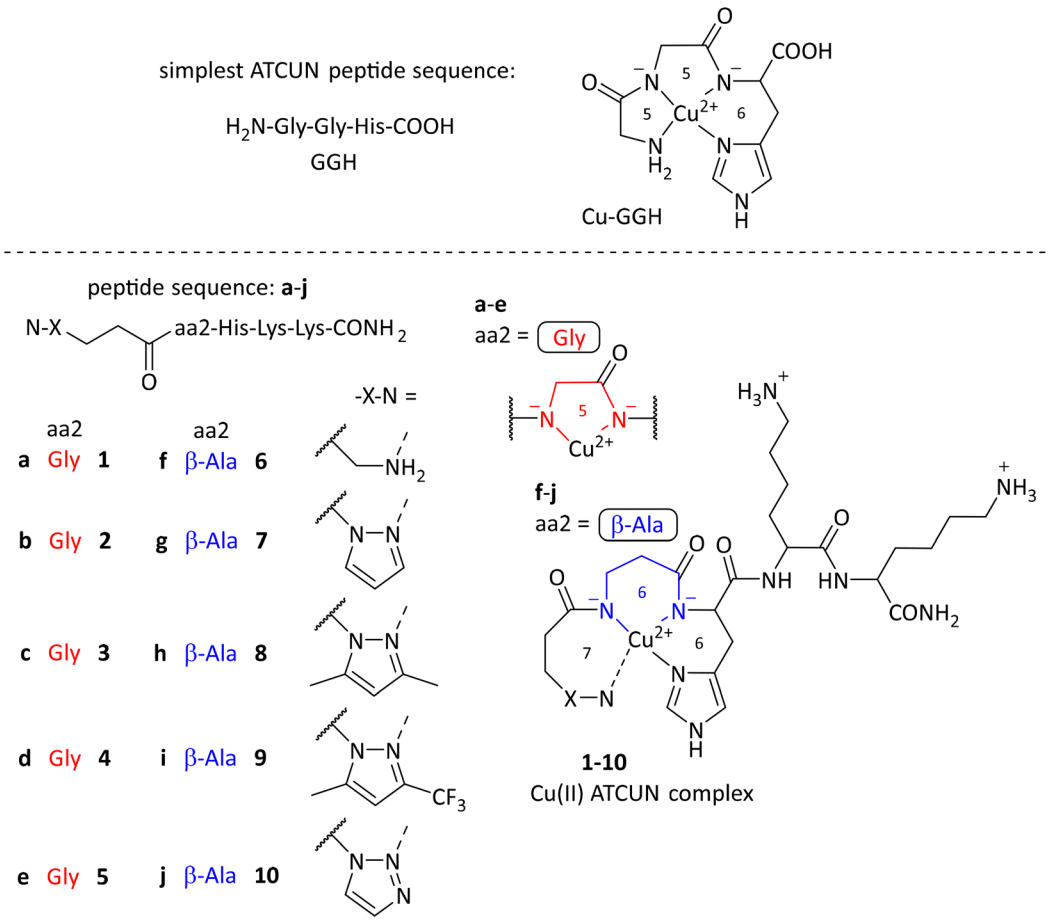

Fig. 1 (Top) Complex structure of the Cu(II) complex Cu-GGH at pH 7.4 with the simplest ATCUN peptide ligand GGH, as originally synthesized by Linus Pauling and coworkers.[20,22] Coordination of GGH to Cu(II) results in chelate rings of different sizes (5,5,6).[20] (Bottom) Cu(II) complexes **1–10** of ATCUN-like peptides **a–j**. The amino acid at the second position (aa2) is either Gly (α-amino acid, 5-membered chelate) or β-Ala (β-amino acid, 6-membered chelate). The N-terminus consists of either γ-aminobutyric acid (GABA), or pyrazolyl propionic acid units with different 3,5-substitutions (CH_3-, CF_3-) or triazolyl propionic acid. Both, incorporation of GABA and pyrazolyl/triazolyl propionic acids results in a 7-membered chelate within the Cu(II) coordination sphere. Peptides **a–j** are amidated, whereas GGH is carboxylated at the C-terminus.

the second position of the peptide sequence (5,5,6 → 5,6,6 chelates) results in a remarkable increase in biological activity *in vitro* (cytotoxicity, ROS generation, DNA cleavage). The additional methylene group in β-Ala (6-membered chelate) facilitated access to the tetrahedral Cu(I) complex geometry, enabling efficient ROS evolution.[29]

In addition, pyrazole-based compounds possess a broad range of biological activities, ranging from antiviral, antifungal, anti-inflammatory, anticancer, and analgesic activities, among others.[30–33] Over the past decades, more than 40 pyrazole-containing drugs have been approved by the FDA (Food and Drug Administration), such as celecoxib[34] (anti-inflammatory) and difenamizole[35] (analgesic) to name only a few, demonstrating the high potential of this compound class for biological applications.[36]

In this work, 3,5-substituted pyrazoles (CF_3-, CH_3-) were introduced at the N-terminus of ATCUN peptides. Whereas the N1 atom of the different pyrazoles was functionalized with 3-propionic acid for solid phase peptide synthesis (SPPS) coupling, the N2 atom provides a Cu(II) binding site. Within the Cu(II) complex structure, incorporation of the pyrazolyl or triazolyl propionic acid moiety at the N-terminus, together with an additional exchange of Gly for β-Ala in the second position results, in different chelate ring systems (7,5,6 and 7,6,6). In addition, positions 4 and 5 of the peptide sequence were elongated with two Lys to increase the positive charge of the complex at pH 7.4.[37] Fig. 1 (bottom) shows the corresponding pyrazole- and triazole-based Cu(II) ATCUN peptide complexes. Here, both the influence of different substituted pyrazoles/triazole at the N-terminus and the increase of the chelate ring sizes (5,5,6 and 5,6,6 as recently reported[29] → 7,5,6 and 7,6,6 respectively) are investigated by *in vitro* ROS generation and DNA cleavage/binding assays to evaluate the biological activity potential. Computational approaches were employed to rationalize the observed bioactivity trends of these synthetic metallopeptides.

Results and discussion

Synthesis and characterization of Cu(II) ATCUN-based peptides complexes

Firstly, the corresponding 3,5-substituted pyrazolyl (CH_3-, CF_3-) and triazolyl 3-propionic acids bearing a carboxyl group for SPPS were synthesized following literature reports.[38,39] Subsequently, the novel ATCUN-like peptides **a–j** were synthesized from L-amino acids and pyrazolyl/triazolyl propionic acids *via* manual solid-phase peptide synthesis (SPPS) using the Fmoc strategy,[40] purified by RP-HPLC, and characterized by ESI-MS and analytical RP-HPLC (S-2). Peptide yields were determined by UV/VIS spectroscopy (S-3). Details can be found in the SI.

Position 2 of the sequence contains either Gly (**a–e**) or β-Ala (**f–j**) to provide a 5- or 6-membered chelate ring within Cu(II) coordination. Additionally, the N-terminus bears either an amine group through GABA coupling in SPPS (**a** and **f**), a 3,5-substituted (CH_3- or CF_3-) pyrazolyl (**b–d** and **g–i**) or a triazolyl unit (**e** and **j**). The N1 atoms of the employed pyrazoles/triazole are functionalized with propionic acid (COOH group for SPPS). Consequently, N2 coordination to Cu(II) ensures the same resulting chelate ring size (*i.e.* 7-membered) as for the N-terminal GABA coupling (see Fig. 1). Thus, starting from the simplest ATCUN motif (GGH) an increase in chelate ring sizes was deliberately designed (5,5,6 → 7,5,6 and 7,6,6, respectively). Lys was attached in positions 4 and 5 of the peptide sequence to facilitate DNA interaction (*vide infra*).

The corresponding Cu(II) ATCUN-like complexes **1–10** (see Fig. 1) were characterized by UV/VIS spectroscopy, mass spectrometry and multi-level computational approaches. The conformational space of complexes **1–10** in their Cu(II) and Cu(I) oxidation states was systematically explored using semi-empirical GFN2-xTB Hamiltonian[41] and the Conformer-Rotamer Ensemble Sampling Tool (CREST).[42] The final structures were re-optimized using tighter convergence criteria. The lowest energy structures were subsequently refined at the DFT level (see SI for details).

The simplest Cu(II) ATCUN complex (5,5,6) exhibits a characteristic d–d transition at around 525 nm.[43] It is known that in Cu(II)-4N peptide complexes an increase in chelate ring size leads to a continuous redshift of the d–d band: 5,5,6 (≈525 nm) → 6,5,6 (≈540 nm) → 5,6,6 (≈555 nm).[37,44] For peptide ligands comprising a potential 6,6,6-based Cu(II) binding motif, a Cu(II)-2N species with a d–d band at 670 nm is observed.[29,37] Incorporation of triazole units at the N-terminus in these 6,6,6-binding peptides neither changes the binding mode nor the d–d transition wavelength of the corresponding complexes (2N, 670 nm), suggesting that the terminal triazolyl arm does not participate in Cu(II) coordination. In contrast, introduction of a pyrazolyl unit at the N-terminus of these 6,6,6-peptide systems results in a Cu(II)-3N or -4N binding mode, which consequently shifts the d–d band to 604 nm.[37]

With this in hand, the UV/VIS spectroscopic features of **1–10** (S-3) can be specified. First, the Gly-containing complexes **1–5** (7,5,6) exhibit their d–d bands in the range of 545–597 nm, whereas the β-Ala complexes **6–10** (7,6,6) show their d–d transitions between 627 and 645 nm. This observation perfectly fits the trend associated with an increase in chelate ring size (*vide supra*; and 7,5,6 → 7,6,6). Since there is no wavelength overlap between these two sets of complexes (Gly: **1–5** *vs.* β-Ala: **6–10**), the binding mode situation within each set is identical: more precisely, independent of the nature of the N-terminus (amine, pyrazole, or triazole) a Cu(II)-3N or Cu(II)-4N binding is suggested, as all complexes **1–10** exhibit d–d bands at wavelengths significantly lower than 670 nm, which is characteristic of a Cu(II)-2N (6,6,6) binding mode; *vide supra*. Moreover, the fact that within each set of complexes (either **1–5** or **6–10**) the wavelength of the d–d transition varies depending on whether the N-terminus is an amine, (substituted) pyrazole, or triazole, suggests that the N-terminal arm – regardless of its specific nature – contributes to Cu(II) coordination, *i.e.* a Cu(II)-4N or -3N binding mode is present. The spectroscopic data discussed here are summarized in Table S4 of the SI.

To corroborate the findings the UV/VIS spectroscopic findings for complexes **1–10**, conformational searches (GFN2-xTB Hamiltonian) and DFT refinement calculations were employed to more clearly identify the Cu binding modes in both the Cu(II) and Cu(I) oxidation states. Square-planar Cu(II) complex starting structures were generated manually, and their conformational flexibility was subsequently explored using CREST in combination with the semiempirical GFN2-xTB Hamiltonian and an implicit solvent model. This approach has been successfully applied to ATCUN complexes.[29,37] Further details are provided in the SI (S-4). After reoptimization at the GFN2-xTB level with tighter convergence criteria, the lowest-energy conformers were refined using density functional theory (DFT) calculations (see SI). For all complexes **1–10**, an ATCUN-based Cu(II)-4N binding mode with a slightly distorted square planar coordination geometry was identified (S-4), as depicted in Fig. 1 for the 7,5,6 and 7,6,6 chelate systems. As representative examples, the DFT re-optimized structures of the global CREST GFN2-xTB minima of the β-Ala complexes **6** (terminal NH_2) and **9** (terminal 3,5-substituted pyrazole, CF_3-, CH_3-) are shown in Fig. 2. In both cases, the characteristic ATCUN-type Cu(II)-4N square planar coordination mode with slight distortion is observed, featuring Cu–N bond lengths of 1.92–2.13 Å, which are typical for stable Cu(II) complexes.[45] All other refined Cu(II) and Cu(I)-ATCUN structures can be found in the SI (Fig. S33–S42). The coordinates of all intermediate conformers (typically between 80 and 329, see Fig. S32) for complexes **1–10** are available in the online repository (see Data Availability Statement).

The lowest energy Cu(II) complex structures were then reduced and the conformational search repeated, followed by a final DFT reoptimization of the global minima. The coordinates of all generated conformers (see Fig. S32) can be found in the repository mentioned in the Data Availability Statement. In contrast to the oxidized Cu(II) species, a different situation is observed for the Cu(I) binding modes of complexes **1–10**.

For the Gly-containing complexes **1**, **4** and **5** and β-Ala complexes **6**, **8** and **9**, a Cu(I)-3N coordination geometry with typical Cu–N bond lengths (1.884–2.217 Å) was identified (S-4). When the weak/elongated bonding of the terminal/imidazole (His) nitrogen to Cu(I) is additionally considered (Cu–N distances of 3.108–5.118 Å), this coordination environment can be regarded as a distorted tetrahedral geometry. For the remaining complexes (Gly: **2** and **3**; β-Ala: **7** and **10**), a Cu(I)-4N binding situation was found, analogous to that observed for the Cu(II) species (*vide supra*). Thus, the calculated Cu(II) complex structures of **1–10** are in excellent agreement with UV/VIS spectroscopic data. No Cu(II)-2N species is present, as evidenced by d–d transitions exclusively below 670 nm, and all Cu(II) complexes **1–10** are dominated by a Cu(II)-4N binding mode. This also implies that all different N-terminal functionalities contribute to Cu(II) coordination in accordance with UV/VIS results showing distinct d–d transition bands within each set (Gly *vs.* β-Ala). In contrast, the corresponding Cu(I) species adopt either Cu(I)-3N or Cu(I)-4N coordination modes.

These findings were corroborated by ESI-MS analysis of complexes **1–10** (S-5). For those complexes in which a Cu-4N coordination mode was computationally identified for both Cu(II) and Cu(I) (Gly: **2** and **3**; β-Ala: **7** and **10**), the ESI-MS results are consistent: both, the Cu(II) and Cu(I) peptide adducts were detected, suggesting that these complexes are the most stable ones. Furthermore, within the two sets of complexes (Gly: **1–5** and β-Ala: **6–10**), compounds **2** and **7** – both bearing an unsubstituted pyrazole at the N-terminus – are the only complexes,

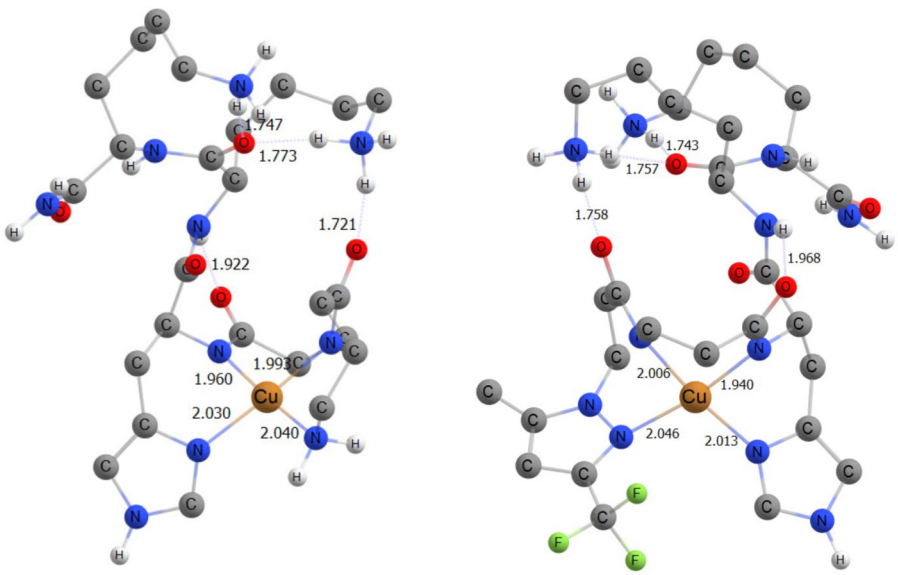

Fig. 2 DFT-refined Cu(II) complex structures of β-Ala compounds **6** (left) with a terminal NH_2 and **9** (right) with a terminal 3,5-substituted (CF_3- and CH_3-) pyrazolyl unit using the GFN2-xTB Hamiltonian and DFT. Hydrogen atoms are not displayed for clarity. For both **6** and **9**, a slightly distorted square planar Cu(II)-4N coordination geometry is present.

for which a 4N-binding is present for both Cu(II) and Cu(I) and for which both oxidation states were detected by ESI-MS. This observation indicates that unsubstituted pyrazolyl termini exert the strongest stabilizing effect, independent of the Cu oxidation state and the amino acid in the second position of the peptide sequence (Gly *vs.* β-Ala). In contrast, the steric hindrance introduced by 3,5-substituted pyrazoles (CF_3- and/or CH_3-) appears to reduce the stability of the 4N coordination mode, favoring a 3N binding situation. This interpretation is fully consistent with the analysis of the number of accessible conformers in both oxidation states. For complexes with unsubstituted pyrazolyl N-termini (Gly complex **2** and β-Ala complex **7**), a comparatively low number of conformers was obtained for both their Cu(II) and Cu(I) species (Fig. S32, for **2**: Cu(II) and Cu(I) < 100 conformers; for **7**: Cu(I) < 100 and Cu(II) ≈ 250), indicating that these complexes are rigidified and strongly coordinating. By contrast, for complexes with a calculated Cu(I)-3N binding (Gly: **1**, **4**, **5** and β-Ala: **6**, **8**, **9**) predominantly only one oxidation stated – either Cu(II) or Cu(I) – was observed in the ESI mass spectra, but not both. This behavior can be rationalized by the higher stability of a chelating 4N coordination mode compared to a 3N complex, as previously reported for related Cu(II) ATCUN-based peptide systems.[20,44] Consequently, the simultaneous detection of both Cu(II) and Cu(I) peptide adducts in ESI-MS follows the expected stability trend (4N > 3N).

DNA cleavage activity

The effect of the different N-termini (amine, (3,5-substituted) pyrazoles, triazole) and various chelate ring sizes (Gly: 7,5,6 *vs.* β-Ala: 7,6,6) on oxidative plasmid DNA cleavage activity was evaluated by gel electrophoresis. The extent of DNA degradation can be monitored by the appearance of different plasmid DNA conformations resulting from increasing numbers of DNA strand breaks: form I (supercoiled) → form II (open circular) → form III (linear).[46] Fig. 3 shows the nuclease activity of *in situ* prepared complexes **1–10** in the presence of $AscH^-$ as a reducing agent (pH 7.4, 37 °C).

First, all complexes **1–10** exhibit nuclease activity in the presence of $AscH^-$ as a reducing agent, indicating an oxidative cleavage mechanism *via* ROS production.[20,37] Amongst the two sets of complexes (Gly (7,5,6): **1–5** *vs.* β-Ala (7,6,6): **6–10**), the activity is slightly higher for the β-Ala complexes. A more flexible ligand scaffold (6- *vs.* 5-membered chelate) facilitates the interconversion between square planar Cu(II) and tetrahedral Cu(I) coordination geometries, which is essential for ROS generation (Scheme 1). This trend (Gly < β-Ala) is consistent with our previous observations.[29,37] Within each set, the nuclease activity varies depending on the nature of the N-terminus, while the overall trend remains consistent between the two series (Gly *vs.* β-Ala) (Fig. 3). Particularly, an amine or a pyrazolyl moiety at the N-terminus (Gly: **1**, **2** and β-Ala: **6**, **7**) display significantly higher DNA cleavage, with 34–89% DNA form III/fragments than their 3,5-substituted (CF_3- and/or CH_3-) or triazolyl analogues (Gly: **3–5** and β-Ala: **8–10**) with 5–19% DNA form III. Furthermore, within the Gly complexes **1–5** the unsubstituted pyrazole complex **2** (7,5,6) has the highest DNA damage ability (79% DNA form III, DNA fragments), whereas in the row of β-Ala complexes the complex **6** with a free amine at the N-terminus (7,6,6) showed the most efficient nuclease activity (89%), even higher than **2**.

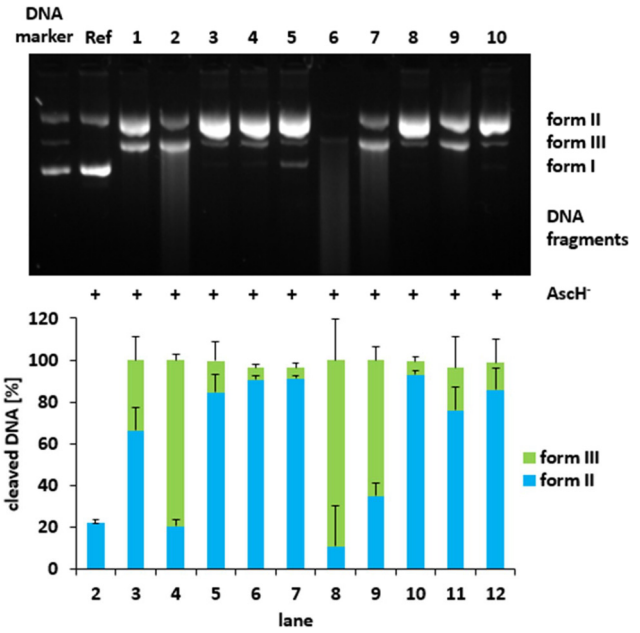

Fig. 3 (Top) Nuclease activity towards plasmid DNA pBR322 (0.2 μg) of Cu(II) ATCUN-based complexes **1–10** (55 μM) in HEPES buffer (50 mM, pH 7.4) in the presence of $AscH^-$ (1 mM) after incubation for 1 h at 37 °C. Lane 1: DNA marker (form I, II and III), lane 2: DNA reference, lanes 3–12 as indicated: **1–10**. (Bottom) Visualization of the extent of DNA cleavage in percent. Error bars represent the standard deviation from at least three experiments.

Thus, regarding DNA cleavage efficiency complex **6** (amine N-terminus; 7,6,6) outperforms Cu(II) ATCUN-based complexes bearing (substituted) pyrazolyl and triazolyl N-terminal functionalities. Furthermore, the observed DNA cleavage activity of complexes **1–10** is within the same range as that of similar metallopeptides.[29,37,43]

Reactive oxygen species

To prove an oxidative DNA cleavage mechanism of complexes **1–10**, a commonly used ROS quenching assay by means of gel electrophoresis[47] was carried out exemplarily using the most potent DNA cleaving agents of each complex set, **2** (Gly, pyrazolyl unit) and **6** (β-Ala, amine). In Fig. 4 the ROS quenching of **6** in the presence of different scavengers (DMSO for $^{\bullet}OH$,[48] NaN_3 for $^1O_2$,[47] pyruvate for H_2O_2 [49] and superoxide dismutase (SOD) for $O_2^{\bullet-}$ [47] is shown. A complex concentration of 52.5 μM, at which DNA forms II and III are more visible (fewer DNA fragments), was chosen.

Firstly, the β-Ala complex **6** showed no DNA cleavage in the absence of $AscH^-$ (*cf.* Fig. 4, lane 10 and lane 2, both ≈25% form II). Consequently, activation through $AscH^-$ is essential for inducing oxidative DNA strand breaks[12] (Scheme 1), which

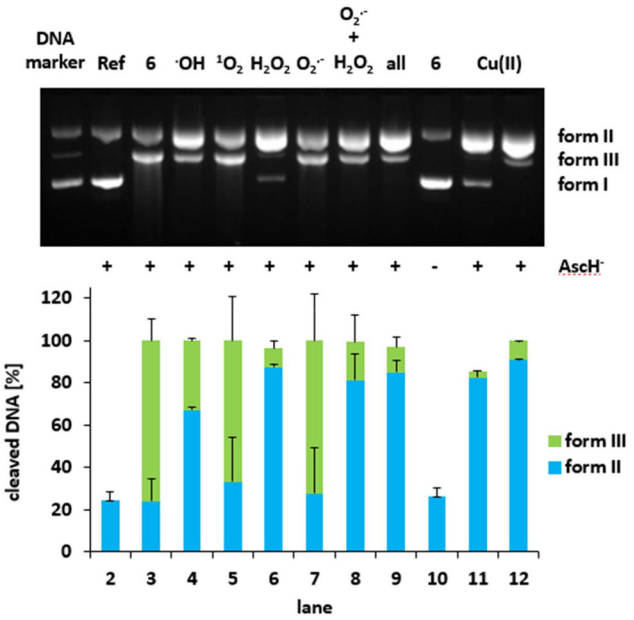

Fig. 4 (Top) Cleavage of plasmid DNA pBR322 (0.2 μg) by complex **6** (52.5 μM) in HEPES buffer (50 mM, pH 7.4) in the presence of $AscH^-$ (1 mM). Incubation for 1 h at 37 °C in the absence and presence of corresponding ROS scavengers. Lane 1: DNA marker (form I, II and III), lane 2: DNA reference, lane 3: **6**, lanes 4–9: **6** and scavengers for the indicated ROS (DMSO (400 mM), NaN_3 (10 mM), pyruvate (2.5 mM), SOD (625 U mL^{-1}), pyruvate (2.5 mM) + SOD (625 U mL^{-1}), all scavengers), lane 10: **6** without $AscH^-$, lane 11: $CuCl_2$ (52.5 μM), lane 12: $CuCl_2$ (55 μM) (Bottom) Visualization of the extent of DNA cleavage in percent. Error bars represent the standard deviation from at least three experiments.

also excludes a hydrolytic DNA damage mechanism.[10,50] In the presence of $AscH^-$, complex **6** (52.5 μM) cleaved plasmid DNA into linear DNA (lane 3: 76% form III). Neither the addition of NaN_3 ($^1O_2$ scavenger) nor SOD ($O_2^{\cdot-}$ scavenger) led to a significant decrease of DNA cleavage (lane 5 and 7: 67 and 73% form III), indicating that these ROS are not involved in the DNA damage process. In contrast, the addition of DMSO and pyruvate strongly reduced the nuclease activity (lane 4 and 6: 32 and 8% form III). Thus, for **6**, $^{\cdot}OH$ and H_2O_2 – formed catalytically as shown in Scheme 1 – are the dominant ROS responsible for DNA cleavage. The same result was obtained by Gly complex **2** (pyrazolyl unit): $^{\cdot}OH$ and H_2O_2 were found to be the generated ROS (S-6: Fig. S53). Hence, independent of the chelate ring sizes (Gly: 7,5,6 *vs.* β-Ala: 7,6,6) or the nature of the N-terminus (amine *vs.* (substituted) pyrazolyl/triazolyl moieties) the same ROS ($^{\cdot}OH$ and H_2O_2) were generated upon $AscH^-$ activation.

Furthermore, since the nuclease activity of $CuCl_2$ at 52.5 μM (lane 11), *i.e.* without peptide ligand, is lower than Cu (II) complexes **6** and **2** (lane 3 and Fig. S53: lane 3), this indicates that the complex structures, as shown in Fig. 1, are the active species (and not unbound Cu(II)) in the used experimental conditions (pH 7.4, 37 °C) (*cf.* also 55 μM $CuCl_2$ (lane 12) and Fig. 3: 55 μM of **1–10**).

Since $^{\cdot}OH$ and H_2O_2 were proven to be involved in DNA cleavage for **2** and **6** exemplarily, a kinetic ROS fluorescence assay was employed to obtain a more detailed assessment of the $^{\cdot}OH$ and H_2O_2 evolution of **1–10**.[29,37] For this purpose, the reaction of terephthalate (TPA) to hydroxyterephthalate (HO-TPA) by $^{\cdot}OH$ and the perhydrolysis of pentafluorobenzenesulfonyl fluorescein (PBSF) into fluorescein by H_2O_2 were monitored by fluorescence spectroscopy.[47] Fig. 5 shows the kinetic production of $^{\cdot}OH$ (TPA → HO-TPA) caused by complexes **1–10**. For the kinetic evolution of H_2O_2 (PBSF → fluorescein) for complexes **1–10** see S-7, Fig. S54.

Firstly, Gly complex **5** (7,5,6) and β-Ala complex **10** (7,6,6) (both 50 μM) exhibit the highest $^{\cdot}OH$ production in this study,

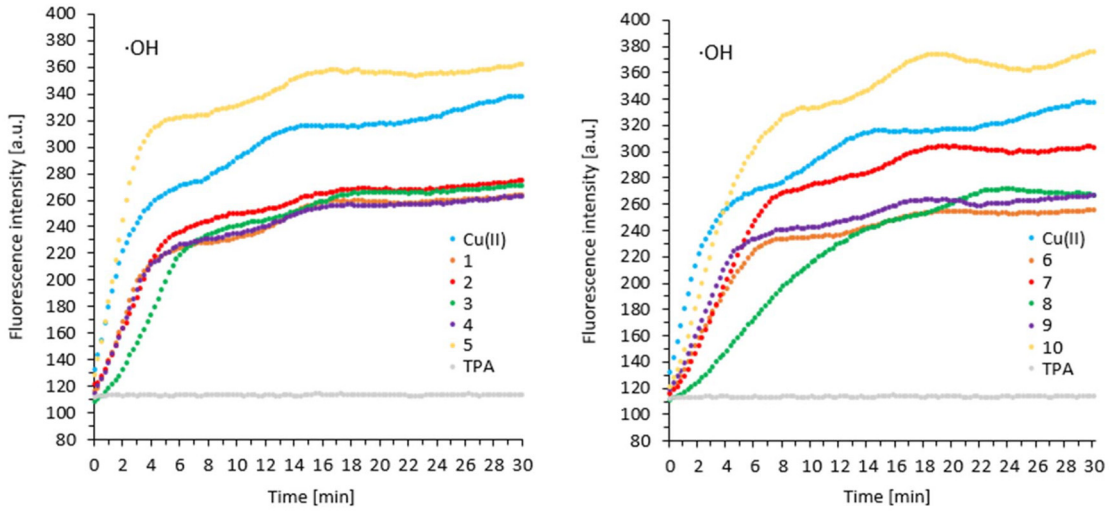

Fig. 5 Kinetics of $^{\cdot}OH$ production for Gly complexes **1–5** (50 μM; left) and β-Ala complexes **6–10** (50 μM; right) in the presence of $AscH^-$ (1 mM) in HEPES buffer (50 mM, pH 7.4) monitored *via* the fluorescence evolution of HO-TPA (λ_{ex} = 320 nm, λ_{em} = 428 nm) over 30 min. In both graphs, identical measurements of $CuCl_2$ (50 μM), denoted as Cu(II), and TPA as negative control (0.5 mM) are included for Gly (7,5,6) *vs.* β-Ala (7,6,6) for reasons of comparison.

even higher than $CuCl_2$. To the best of our knowledge, this represents for the first observation of such pronounced $^{\bullet}OH$ generation for ATCUN-based metallopeptides. Thus, independent of whether a 7,5,6 or 7,6,6 chelate system is present, a triazolyl N-terminus leads to an unprecedented increase of $^{\bullet}OH$ production. This observation is in good agreement with the high number of conformers found for **5** *via* CREST (Fig. S32: for Cu(II) ≈ 200 and Cu(I) ≈ 600, the highest values within Gly complex series), which correlates with increased ligand flexibility and facilitates efficient ROS generation through enhanced interconversion between square planar Cu(II) and tetrahedral Cu(I) geometries (Scheme 1).[29] Although H_2O_2 evolution of complexes **5** and **10** is only moderate (see S-7: Fig. S54), their $^{\bullet}OH$ production is highly efficient (Fig. 5). These findings indicate rapid catalytic ROS generation, in O_2 is converted *via* H_2O_2 as short-lived intermediate to $^{\bullet}OH$. Notably, despite their efficient $^{\bullet}OH$ production, the DNA cleavage activity of complexes **5** and **10** is only moderate compared to the other complexes (Fig. 3: lane 7 and 12), a behavior that is discussed in the context of DNA binding affinity below (*vide infra*).

Surprisingly, for the most efficient DNA cleaving agent **6** (amine group; 7,6,6) followed by **2** (pyrazolyl unit; 7,5,6) the kinetic generation of both H_2O_2 and $^{\bullet}OH$ is comparatively moderate (*cf.* Fig. 5 and S54), with ROS generation of **2** even exceeding that of **6**. Thus, the enhanced nuclease activity of **2** and **6** (Fig. 3, **6** > **2**) does not directly correlate with their *in situ* ROS generation (here: **6** < **2**). This apparent discrepancy can be rationalized by the superior DNA binding properties of **6**, as discussed below (*vide infra*).

Regarding the 3,5-substituted (CF_3-, CH_3-) pyrazolyl complexes **3**, **4** (7,5,6) as well as **8** and **9** (7,6,6), ROS generation ($^{\bullet}OH$ and H_2O_2) is comparatively low to moderate – especially for **8** with respect to $^{\bullet}OH$ formation (Fig. 5 and S54). This behavior is in accordance with their weak to moderate DNA cleavage activities, and reduced DNA binding affinities (*vide infra*). Notably, although for complexes **8** and **9** the largest degree of conformational flexibility (≈250–400 conformers for Cu(II) and Cu(I)) was found, which would typically favor ROS generation, this enhanced flexibility does not translate into increased ROS generation under the applied experimental conditions. We suggest that the absence of enhanced conformational flexibility upon reduction may be one issue here.

DNA binding interactions

It is known that metal complexes can bind to DNA by either intercalation (planar molecules inserted between the aromatic nucleobases of DNA *via* π–π stacking), minor or major groove binding, and/or electrostatic interactions of positively charged metal complexes with the negatively charged phosphate backbone of DNA.[51]

Since, for some complexes (*e.g.* **2**, **5**, **6**, and **10**) in this work the DNA cleavage ability does not correlate with their ROS generation, while for others it does (*e.g.* **3**, **4**, **8**, and **9**), DNA binding studies were conducted to obtain a comprehensive understanding of the observed biological activity trends. For this purpose, three complementary DNA binding assays were employed (S-8): (i) an ethidium bromide (EtBr) displacement assay monitored by fluorescence spectroscopy to determine apparent DNA binding constants (K_{app}),[52] (ii) DNA melting temperature measurements *via* UV/VIS spectroscopy (ΔT_m),[53] and (iii) circular dichroism (CD) spectroscopy.[54] The results are summarized in Table 1.

All complexes **1–10** bear a positively charged Lys–Lys tail (see Fig. 1, the amine groups of the Lys side chains are protonated at pH 7.4 [29,37]). Consequently, all complexes exhibit at least electrostatic interactions with the negatively charged DNA phosphate backbone. Overall, the DNA binding modes differ among complexes **1–10** (see Table 1). Furthermore, the DNA binding strength of complexes **1–10** can generally be classified as moderate, since the CD spectra of CT-DNA do not change significantly upon addition of the corresponding complexes (S-8.3), and the determined K_{app} and ΔT_m values indicate predominantly electrostatic interaction and/or groove binding character ($K_{app} \leq 10^5$ M^{-1} and $\Delta T_m \leq 3.2$ °C).[29,37,55,56] For the β-Ala complexes **6–10** (7,6,6) partial intercalation is additionally observed ($K_{app} = 10^6$ M^{-1}), which is in accordance with the CD spectroscopic data (small changes of the positive CD band at 275 nm, S-8.3). The (substituted) pyrazole and triazole units owing to their planar structures, can promote intercalative

Table 1 DNA binding results of complexes **1–10** and $CuCl_2$ towards calf thymus (CT) DNA as determined by EtBr displacement assay (K_{app} values), DNA melting temperature shifts (ΔT_m) and CD spectroscopy

Compound	K_{app} [M^{-1}]	ΔT_m [°C]	DNA interactions *via* CD spectroscopy[a]
1	5.40×10^5	3.2 ± 0.1	Weak groove binding
2	1.40×10^5	2.2 ± 1.0	—
3	1.50×10^5	1.4 ± 0.9	—
4	3.29×10^5	3.7 ± 0.1	Weak intercalation
5	1.21×10^6	2.5 ± 0.6	Weak intercalation
6	2.44×10^6	5.0 ± 0.4	Partial intercalation, groove binding
7	1.29×10^6	2.8 ± 0.4	Weak intercalation, weak groove binding
8	1.09×10^6	2.2 ± 0.8	Weak intercalation, weak groove binding
9	1.33×10^6	2.5 ± 1.1	Weak intercalation, weak groove binding
10	2.56×10^6	1.1 ± 0.2	Weak intercalation, weak groove binding
$CuCl_2$	3.33×10^5	2.0 ± 1.0	Weak intercalation

[a] Since electrostatic DNA interactions do not alter the CD spectrum of CT-DNA,[29] this binding mode for **1–10** and $CuCl_2$ is not mentioned.

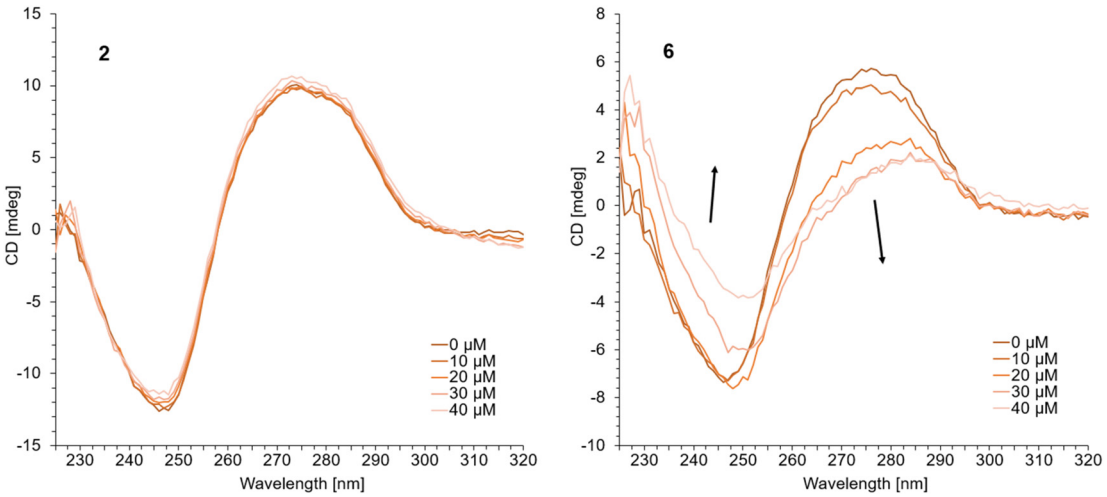

Fig. 6 CD spectra of CT-DNA (100 μM) in HEPES buffer (50 mM, pH 7.4) at 37 °C with increasing concentrations (0–40 μM) of Gly complex **2** (left) and β-Ala complex **6** (right).

binding, which appears to be more pronounced for β-Ala 7,6,6 systems.

Most notably, the most efficient DNA-cleaving agent in this study, complex **6** (β-Ala, N-terminal amine) exhibits comparatively low ROS generation (*vide supra*). In contrast, complex **2** (Gly, unsubstituted pyrazolyl unit) displays enhanced hydroxyl radical formation, but only moderate DNA cleavage activity (*vide supra*). These observations can be rationalized by their distinct DNA binding properties. Complex **6** exhibits an exceptionally strong DNA binding affinity, with a K_{app} value of 2.44×10^6 M^{-1} and ΔT_m of 5.0 ± 0.5 °C, both indicative of partial intercalation.[29,55–57] In addition, it induces the most pronounced alterations in the CD spectrum of CT-DNA, affecting both the positive band (intercalation) and the negative band (groove binding) (Fig. 6, right). This strong DNA interaction likely accounts for its high DNA cleavage activity despited only moderate ROS generation. In contrast, complex **2** shows comparatively weak DNA binding characterized by purely electrostatic interactions in all three assays: $K_{app} = 1.40 \times 10^5$ M^{-1}, $\Delta T_m = 2.2 \pm 1.0$ °C and no alterations in the CD spectrum of CT-DNA (Fig. 6, left).[29,37] Consequently, despite it enhanced ROS production, complex **2** exhibits only moderate DNA cleavage activity.

Insights from calculations further support these findings. In the Cu(I) structure of complex **6** (Fig. S38), the planar imidazole ring of the His residue is no longer coordinating the metal center (Cu–N 5.12 Å), rendering it more accessible for intercalative DNA interactions. Such labile His coordination was not observed for any other complex investigated here, in either the Cu(II) or and Cu(I) oxidation state (*cf.* S-4 and Fig. 2). This structural feature likely contributes to the enhanced DNA binding and cleavage efficiency observed for complex **6**.[58]

Notably, for the efficient hydroxyl radical-generating complexes **5** and **10** (both bearing N-terminal triazolyl moieties in 7,5,6- and 7,6,6-chelates) exhibit comparatively low DNA cleavage activity. This observation would suggest weak DNA binding as a possible explanation. However, considering all three DNA-binding assays, complexes **5** and **10** do not display weak but rather moderate DNA binding affinities, despite their relatively high K_{app} values.

Conclusion

Since the discovery of the anticancer activity and DNA cleavage ability of the simplest Cu(II) ATCUN complex (Gly–Gly–His; 5,5,6-chelate system) in 1983, no substantial improvement in biological activity through structural modifications of the Cu(II) complex had been achieved over the past four decades. This stagnation led to a decline in interest in ATCUN-based Cu(II) complexes as potential therapeutic agents.[28] Recently, we demonstrated that incorporation of β-Ala in such Cu(II) ATCUN complexes (5,5,6 → 5,6,6) significantly enhances ROS generation, and, consequently, DNA cleavage activity.[29]

In the present work, we investigated the influence of 7,5,6- and 7,6,6-chelate rings (Gly *vs.* β-Ala in the second position of the peptide ligand), in combination with 3,5-substituted (CF_3-, CH_3-) pyrazolyl and triazolyl moieties at a 7-membered N-terminus on their biological activity including ROS generation, DNA-cleavage, and DNA binding. We demonstrate that an unsubstituted pyrazolyl moiety in a 7,5,6-ATCUN-based Cu(II) complex (complex **2**) leads to enhanced $^{\bullet}OH$ generation, but only moderate DNA cleavage due to its comparatively weak DNA binding affinity. In contrast, incorporation of a simple amine group at the N-terminus (*via* GABA) in a 7,6,6-ATCUN Cu(II) complex (complex **6**) results in the highest nuclease activity among all studied complexes, which can be attributed to its exceptional DNA binding capability. Furthermore, N-terminal modification with a triazolyl moiety – independent of the chelate ring system (7,5,6 in complex **5** or 7,6,6 in complex **10**) – leads to pronounced hydroxyl radical formation. Overall, the observed biological activities of complexes **1–10**

with respect to DNA cleavage/binding and ROS generation are within the range reported for similar metallopeptides, including those bearing Lys–Lys tails.[20,25,29,37,43,59]

In conclusion, the combination of 7,5,6- or 7,6,6-chelate motifs in Cu(II) ATCUN complexes with N-heterocyclic (pyrazoles or triazole) or amine N-termini represents a powerful strategy to restore and enhance the biological activity of otherwise weakly active ATCUN-based systems. These findings advance ATCUN-derived metallopeptides towards potential applications in medicinal chemistry and biotechnology.

Conflicts of interest

There are no conflicts to declare.

Data availability

The experimental data supporting this article have been included as part of the supplementary information (SI). Supplementary information: materials and general methods, synthesis of peptides and complexes, DNA binding and cleavage studies. See DOI: https://doi.org/10.1039/d6dt00630b.

The computational results and data are available in the open repository EDMOND. See https://doi.org/10.17617/3.LBNPK2.

Acknowledgements

The authors thank Otto von Guericke University and the University of Potsdam for financial support. D. V. thanks the GRIAT program for funding. R. K. is supported by a Max-Planck-Weizman postdoctoral fellowship. M. S. is grateful to the Max Planck Society for the Advancement of Science. N. K. and M. S. thank the Ministry for Science, Energy, Climate Protection and the Environment of the State of Saxony-Anhalt for support within 'SmartProSys: Intelligent Process Systems for the Sustainable Production of Chemicals' and the 'OVGU Research Center Dynamic Systems' (European Regional Development Fund–ERDF grant ZS/2016/04/78155). The authors thank Marcel Kühling and Dr Phil Köhler for support with the pyrazole derivatives synthesis.

References

1 B. D. Ellenbroek, J. P. Kahler, S. R. Evers and S. J. Pomplun, *Angew. Chem., Int. Ed.*, 2024, **63**, e202401704.
2 Z. Yu and J. A. Cowan, *Curr. Opin. Chem. Biol.*, 2018, **43**, 37–42.
3 M. Yousefzadeh, C. Henpita, R. Vyas, C. Soto-Palma, P. Robbins and L. Niedernhofer, *eLife*, 2021, **10**, e62852.
4 P. Majtnerová and T. Roušar, *Mol. Biol. Rep.*, 2018, **45**, 1469–1478.
5 M. Galanski, M. A. Jakupec and B. K. Keppler, *Curr. Med. Chem.*, 2005, **12**, 2075–2094.
6 C.-L. Zhao, X. Qiao, X.-M. Liu, X.-Q. Song, Y.-H. Zou, D.-Q. Li, X.-W. Yu, W.-G. Bao and J.-Y. Xu, *Eur. J. Pharmacol.*, 2022, **925**, 174985.
7 N. A. G. dos Santos, R. S. Ferreira and A. C. dos Santos, *Food Chem. Toxicol.*, 2020, **136**, 111079.
8 R. L. Lucaciu, A. C. Hangan, B Sevastre and L. S. Oprean, *Molecules*, 2022, **27**, 6485.
9 K. Ni, N. Montesdeoca and J. Karges, *Dalton Trans.*, 2024, **53**, 8223–8228.
10 C. Wende, C. Lüdtke and N. Kulak, *Eur. J. Inorg. Chem.*, 2014, 2597–2612.
11 C. Santini, M. Pellei, V. Gandin, M. Porchia, F. Tisato and C. Marzano, *Chem. Rev.*, 2014, **114**, 815–862.
12 E. Falcone, V. Vigna, H. Schueffl, F. Stellato, B. Vileno, M. Bouraguba, G. Mazzone, O. Proux, S. Morante, P. Heffeter, E. Sicilia and P. Faller, *Angew. Chem., Int. Ed.*, 2024, e202414652.
13 G. Pizzino, N. Irrera, M. Cucinotta, G. Pallio, F. Mannino, V. Arcoraci, F. Squadrito, D. Altavilla and A. Bitto, *Oxid. Med. Cell. Longevity*, 2017, 8416763.
14 R. Hakem, *EMBO J.*, 2008, **27**, 589–605.
15 Q. Jiang, N. Xiao, P. Shi, Y. Zhu and Z. Guo, *Coord. Chem. Rev.*, 2007, **251**, 1951–1972.
16 M. Anjomshoa and B. Amirheidari, *Coord. Chem. Rev.*, 2022, **458**, 214417.
17 C. Harford and B. Sarkar, *Acc. Chem. Res.*, 1997, **30**, 123–130.
18 G. Gasmi, A. Singer, J. Forman-Kay and B. Sarkar, *J. Pept. Res.*, 1997, **49**, 500–509.
19 K. L. Haas, A. B. Putterman, D. R. White, D. J. Thiele and K. J. Franz, *J. Am. Chem. Soc.*, 2011, **133**, 4427–4437.
20 P. Gonzalez, K. Bossak, E. Stefaniak, C. Hureau, L. Raibaut, W. Bal and P. Faller, *Chem. – Eur. J.*, 2018, **24**, 8029–8041.
21 T. Frączyk, *Chem. Biodiversity*, 2021, **18**, e2100043.
22 E. Kimoto, H. Tanaka, J. Gyotoku, F. Morishige and L. Pauling, *Cancer Res.*, 1983, **43**, 824–828.
23 S. H. Chiou, *J. Biochem.*, 1983, **94**, 1259–1267.
24 C. M. Agbale, M. H. Cardoso, I. K. Galyuon and O. L. Franco, *Metallomics*, 2016, **8**, 1159–1169.
25 J. A. Cowan, *Pure Appl. Chem.*, 2008, **80**, 1799–1810.
26 Z. Yu, M. Han and J. A. Cowan, *Angew. Chem., Int. Ed.*, 2015, **54**, 1901–1905.
27 A. Santoro, G. Walke, B. Vileno, P. P. Kulkarni, L. Raibaut and P. Faller, *Chem. Commun.*, 2018, **54**, 11945–11948.
28 J. Heinrich, E. Siddiqui, H. Eckstein, M. Naumann and N. Kulak, *J. Biol. Inorg. Chem.*, 2024, **29**, 801–809.
29 J. Heinrich, K. Bossak-Ahmad, M. Riisom, H. H. Haeri, T. R. Steel, V. Hergl, A. Langhans, C. Schattschneider, J. Barrera, S. M. F. Jamieson, M. Stein, D. Hinderberger, C. G. Hartinger, W. Bal and N. Kulak, *Chem. – Eur. J.*, 2021, **27**, 18093–18102.
30 F. K. Keter and J. Darkwa, *BioMetals*, 2012, **25**, 9–21.
31 O. Ebenezer, M. Shapi and J. A. Tuszynski, *Biomedicines*, 2022, **10**, 1124.

32 A. Ansari, A. Ali, M. Asif and Shamsuzzaman, *New J. Chem.*, 2017, **41**, 16–41.
33 Ş. G. Küçükgüzel and S. Şenkardeş, *Eur. J. Med. Chem.*, 2015, **97**, 786–815.
34 P. L. McCormack, *Drugs*, 2011, **71**, 2457–2489.
35 R. Kumar, R. Sharma and D. K. Sharma, *Curr. Top. Med. Chem.*, 2023, 232098–232115.
36 G. Li, Y. Cheng, C. Han, C. Song, N. Huang and Y. Du, *RSC Med. Chem.*, 2022, **13**, 1300–1321.
37 J. Barrera, H. H. Haeri, J. Heinrich, M. Stein, D. Hinderberger and N. Kulak, *Dalton Trans.*, 2023, **52**, 3279–3286.
38 P. Liebing and F. T. Edelmann, *Helv. Chim. Acta*, 2020, **103**, e2000148.
39 A. Williams, *J. Am. Chem. Soc.*, 1976, **98**, 5645–5651.
40 R. Behrendt, P. White and J. Offer, *J. Pept. Sci.*, 2016, **22**, 4–27.
41 C. Bannwarth, S. Ehlert and S. Grimme, *J. Chem. Theory Comput.*, 2019, **15**, 1652–1671.
42 P. Pracht, F. Bohle and S. Grimm, *Phys. Chem. Chem. Phys.*, 2020, **22**, 7169–7192.
43 Y. Jin and J. A. Cowan, *J. Am. Chem. Soc.*, 2005, **127**, 8408–8415.
44 J. Nagaj, K. Stokowa-Sołtys, I. Zawisza, M. Jeżowska-Bojczuk, A. Bonna and W. Bal, *J. Inorg. Biochem.*, 2013, **119**, 85–89.
45 Y. J. Lee, Y. Kim, H. Kim, J. Choi, G. H. Noh, K.-S. Lee, J. Lee, C. H. Choi, S. H. Kim and J. Seo, *Inorg. Chem.*, 2023, **62**, 10279–10290.
46 T. Schwarze, M. Al Akrami, J. Heinrich, V. Hergl, E. Sperlich, A. Kelling, T. Sprenger, N. Jahn, T. Klamroth and N. Kulak, *Phys. Chem. Chem. Phys.*, 2025, **27**, 24178–24183.
47 S. Leichnitz, J. Heinrich and N. Kulak, *Chem. Commun.*, 2018, **54**, 13411–13414.
48 M. K. Eberhardt and R. Colina, *J. Org. Chem.*, 1988, **53**, 1071–1074.
49 E. A. Mazzio and K. F. A. Soliman, *Neurochem. Res.*, 2003, **28**, 733–741.
50 E. L. Hegg and J. N. Burstyn, *Coord. Chem. Rev.*, 1998, **173**, 133–165.
51 B. J. Pages, D. L. Ang, E. P. Wright and J. R. Aldrich-Wright, *Dalton Trans.*, 2015, **44**, 3505–3526.
52 X. Sheng, X.-M. Lu, Y.-T. Chen, G.-Y. Lu, J.-J. Zang, Y. Shao, F. Liu and Q. Xu, *Chem. – Eur. J.*, 2007, **13**, 9703–9712.
53 J. Wang, X. Pan and X. Liang, *J. Anal. Methods Chem.*, 2016, **2016**, 5318935.
54 V. I. Ivanov, L. E. Minchenkova, A. K. Schyolkina and A. I. Poletayev, *Biopolymers*, 1973, **12**, 89–110.
55 S. Roy, A. K. Patra, S. Dhar and A. R. Chakravarty, *Inorg. Chem.*, 2008, **47**, 5625–5633.
56 X. Sheng, X.-M. Lu, Y.-T. Chen, G.-Y. Lu, J.-J. Zhang, Y. Shao, F. Liu and Q. Xu, *Chem. – Eur. J.*, 2007, **13**, 9703–9712.
57 V. Behling, J. Heinrich, D. Díaz, E. H. P. Brohmer, J. Heinrich, N. Schlörer, S. Kupfer, N. Kulak and P. Köhler, *Dalton Trans.*, 2025, **54**, 12772–12783.
58 A. Arunadevi, R. Paulpandiyan and N. Raman, *J. Mol. Liq.*, 2017, **241**, 801–810.
59 B. K. Maiti, N. Govil, T. Kundu and J. J. G. Moura, *iScience*, 2020, **23**, 101792.